

# On the optical conductivity of Electron-Doped Cuprates I: Mott Physics

A. J. Millis<sup>1</sup>, A. Zimmers<sup>2,3</sup>, R. P. S. M. Lobo<sup>2</sup>, N. Bontemps<sup>2</sup>

<sup>(1)</sup> *Department of Physics, Columbia University  
534 W. 120th St. New York, N. Y. 10027*

<sup>(2)</sup> *LPS-ESPCI, CNRS UPR 5,  
10 rue Vauquelin, 75231, Paris Cedex 5, France*

<sup>(3)</sup> *Center for Superconductivity Research  
University of Maryland, College Park, MD 20742*

The doping and temperature dependent conductivity of electron-doped cuprates is analysed. The variation of kinetic energy with doping is shown to imply that the materials are approximately as strongly correlated as the hole-doped materials. The optical spectrum is fit to a quasiparticle scattering model; while the model fits the optical data well, gross inconsistencies with photoemission data are found, implying the presence of a large, strongly doping dependent Landau parameter.

PACS numbers: 74.72-h, 71.27+a, 74.25.Gz

## I. INTRODUCTION

Despite 15 years of intensive study many properties of the cuprate superconductors remain imperfectly understood. A crucial set of questions involves charge transport. Angle resolved photoemission measurements<sup>1</sup> suggest the presence of reasonably well defined electron-like quasiparticle excitations characterized by a Fermi surface with position very close to that of band theory and a quasiparticle velocity only moderately renormalized from the band value. Optical measurements reveal a frequency dependent conductivity<sup>2,3</sup> with a strong doping dependence and an integrated low frequency absorption strength ("spectral weight") markedly smaller than that predicted by band theory<sup>4</sup>.

There is no generally accepted interpretation of the measured conductivity of high- $T_c$  cuprates. Some authors argue that it may be understood in terms of quasiparticles scattered by a frequency and temperature dependent scattering rate<sup>2,5,6</sup>; others that it should be understood in more exotic terms<sup>7,8</sup>. Recently, the issue of the adequacy of a quasiparticle-only description has been reexamined<sup>9</sup>. For hole-doped materials at optimal doping a model involving only quasiparticles with velocity and mean free path taken from angle-resolved photoemission experiments, was shown to be inconsistent with the data.

A suppression of low frequency optical oscillator strength is expected in materials, such as the high  $T_c$  superconductors, which may be regarded as doped Mott insulators. Our understanding of the physics of doped Mott insulators is far from complete. However, the development over the last 15 years of the 'dynamical mean field method' has provided an important theoretical step forward<sup>10</sup>, providing a practical (and in many cases apparently reliable) method for calculating properties of strongly correlated materials and leading to new insights into the one-electron (photoemission and specific heat) properties of doped Mott insulators<sup>11</sup>. A crucial assumption in this method is that the electron self energy depends much more strongly on energy than on momentum.

This assumption may be theoretically justified in a limit of infinite spatial dimensionality. It implies that 'vertex corrections' may be neglected, making the calculation of the optical conductivity straightforward once the electron self energy has been determined. In other words, the key consequence of this theoretical approach is that the Mott correlations are expressed mainly through the electron self energy, and in particular the suppression of low frequency spectral weight occurring as the Mott phase is approached is caused by a divergence of the electron effective mass. An alternative class of theoretical approaches<sup>12</sup> involves ascribing the Mott spectral weight suppression to a 'vertex correction' which diverges as the insulating phase is approached.

The experimental status of these predictions is unsettled. Good agreement between dynamical mean field calculations and data has been found for electronically three dimensional compounds such as  $V_2O_3$ <sup>13</sup>. However, the applicability of the method to two dimensional correlated materials is not clear. The discrepancies between the quasiparticle-only model and BSCCO optical data were interpreted by<sup>9</sup> as implying the presence of a relatively large vertex correction, but the evolution of the vertex correction with doping was not determined because only for optimally doped BSCCO were a consistent set of photoemission and optical data available. One implementation of the vertex correction idea, the slave-boson-gauge theory approximation<sup>12</sup> has a reasonable qualitative correspondence with the measured conductivity, but has been shown to make predictions for the doping and temperature dependence of the superconducting penetration depth which disagree sharply with data<sup>14</sup>.

Recent experimental developments may offer a new perspective on the charge dynamics of high temperature superconductors and therefore of low dimensional Mott insulators. Improvements in sample preparation have led to a systematic set of measurements on *electron-doped* cuprate materials<sup>15,16,17</sup>. The electron-doped compounds, unlike the more extensively studied hole-doped compounds, display at  $x \leq x = 0.15$  and low enough temperature clear signatures of a density wave gap in

the observed conductivity<sup>15,16,17</sup>. Recent theoretical works<sup>18,19</sup> have explained the difference in magnetic behavior between electron-doped and hole-doped compounds in terms of a model in which the electron-doped compounds exhibit 'Mott' correlations which are weaker than in the hole-doped ones, and are doping dependent.

In this paper we undertake a systematic analysis of the observed conductivity of the electron doped materials. Measurements at lower temperatures and lower dopings reveal gap-like features which may be associated with antiferromagnetic order<sup>16,17</sup>. We consider data only at dopings and temperatures such that the density wave gap effects do not affect the analysis; a companion paper reports results of more detailed studies of density wave gap effects. We show that the magnitude and doping dependence of the kinetic energy implies that the electron-doped cuprates are approximately as strongly correlated as the hole-doped compounds. We further show that the canonical model of quasiparticles scattered by a (possibly large) self energy is an entirely inadequate description of the data. The rest of this paper is organized as follows. In section II we define the model and the quantities of interest. Section III presents the specific form of the self energy used in our detailed analysis. Section IV presents an analysis of the qualitative features of the conductivity, in particular the kinetic energy and optical mass enhancement. Section V presents an attempt to model the conductivity under the 'no-vertex-corrections' approximation using the self energy presented in section III. Section VI outlines implications for the photoemission spectra and section VII is a conclusion.

## II. MODEL

### A. Overview

The conventional description of the motion of electrons in solids is in terms of electrons, moving with a dispersion defined by a band structure calculation and modified by a self energy function expressing the effects of interactions not included in the band calculation. In this section we present the band structure which seems likely to be relevant to the materials, and define the optical conductivity and related quantities including the 'kinetic energy' which is a fundamental measure of the correlation strength of the materials.

### B. Band Structure

The canonical band structure of high- $T_c$  materials<sup>20</sup> is

$$\begin{aligned} \varepsilon_p = & -2t_1 (\cos p_x + \cos p_y) + 4t_2 \cos p_x \cos p_y \\ & - 2t_3 (\cos 2p_x + \cos 2p_y) \end{aligned} \quad (1)$$

The parameters  $t_1, t_2, t_3$  have been obtained from band theory calculations for *hole-doped* compounds by a 'down-

folding' procedure<sup>20</sup>; canonical values are

$$t_1 = 0.38eV \quad (2)$$

$$t_2 = 0.32t_1 \quad (3)$$

$$t_3 = 0.5t_2 \quad (4)$$

The Fermi surface found in band theory calculations performed directly on electron-doped materials<sup>21</sup> is almost identical to the Fermi surface following from Eq 1.

For the energy dispersion implied by these parameters, at all relevant carrier concentrations the Fermi surface is hole-like (roughly circular, centered at the  $\pi, \pi$  point). The Fermi surface implied by Eq 1 for electron-doping of  $x = 0.17$  is shown as the solid line in Fig 1 overlaid on a false-color representation of the experimental near-fermi-surface photoemission intensity<sup>22</sup>. In this measurement the fermi surface is in the lighter-shaded. (Other very recent measurements have found a slightly different shape<sup>23</sup>, the differences are too small to be relevant to the present paper).

Note that although the correspondence between the calculated and measured Fermi surfaces is not perfect, it is reasonably good. Note also that the area enclosed by the calculated curve is equal to that enclosed by the measured one, suggesting that the actual doping of the region measured in the experiment is slightly higher than the nominal doping of  $x = 0.15$ . The strong similarity between the calculation and the data appears to rule out the possibility of gross differences in the underlying Fermiology between hole-doped to electron-doped materials, in particular contradicting the theoretical suggestion<sup>24</sup> that many-body physics effects could lead to a change in sign of  $t_2$  between electron and hole-doped materials. We believe that the agreement between the observed Fermi surface and the band theory one justifies the use of the tight-binding parameters in modelling the optical data.

In wide classes of 'correlated electron' materials, standard band theory calculations produce Fermi surfaces in reasonable agreement with experiment; however, electronic dispersions are often substantially renormalized. Fig 2 compares the dispersion obtained from angle-resolved photoemission measurements along two high-symmetry directions in the Brillouin zone, to those obtained from the simple tight binding parameters used above. One sees that in both symmetry directions the measured velocities are roughly half of the band velocities.

### C. Optical conductivity

The optical conductivity  $\sigma(\Omega)$  is the response function relating current to applied uniform, transverse electric field; it is given by

$$\sigma(\Omega) = \frac{e^2}{i\Omega} \int dt e^{-i\Omega t} \langle [\vec{j}(t), \vec{j}(0)] \rangle \quad (5)$$

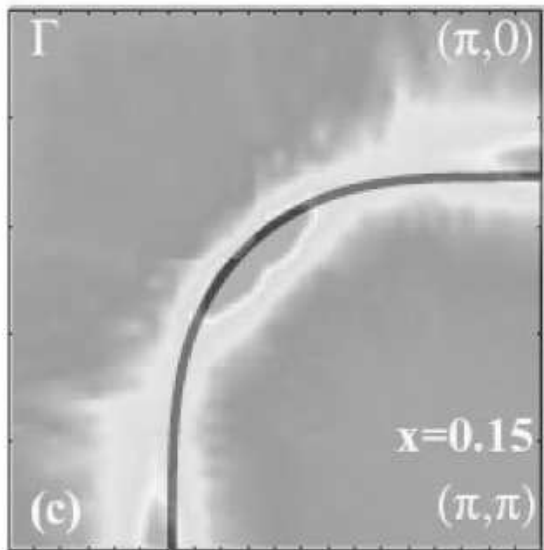


FIG. 1: Solid line: Fermi surface of electron doped cuprates at  $x = 0.17$  calculated from Eq 1 using the standard band parameters given in the text and overlaid on a false-color representation of the near-chemical-potential photoemission intensity<sup>22</sup> derived from angle resolved photoemission measurements of an NCCO sample with nominal electron-doping  $x = 0.15$ . In this measurement the Fermi surface is located in the light-shaded region.

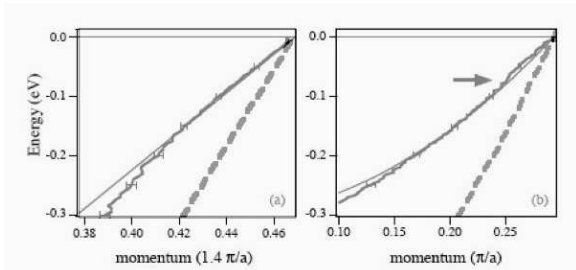


FIG. 2: Observed quasiparticle dispersions (solid lines) from angle resolved photoemission measurements on  $Nd_{1.85}Ce_{0.15}CuO_4$ <sup>22</sup> compared to tight binding model prediction (dashed lines). Panel a: zone diagonal ( $(0,0) \rightarrow (\pi,\pi)$ ); Panel (b) zone face ( $(\pi,0) \rightarrow (\pi,\pi)$ ).

At frequencies below interband transitions the current operator  $\vec{j}$  is  $\vec{j} = \partial\varepsilon_p/\partial\vec{p}$ . In the matrix notations of the preceding section, the operator for current flow in the  $x$  direction is

$$\mathbf{j}_x = \frac{\partial\varepsilon_p}{\partial p_x} \quad (6)$$

explicitly,

$$j_{x,p} = \frac{\partial\varepsilon_p}{\partial p_x} = 2t_1 \sin p_x - 4t_2 \sin p_x \cos p_y + 4t_3 \sin 2p_x \quad (7)$$

and we have chosen units such that the in-plane lattice constant is unity.

An important aspect of the conductivity is the spectral weight, or integrated area, which is most conveniently expressed as an energy via

$$K(\Omega) = \frac{\hbar c}{e^2} \int_0^\Omega \frac{2d\omega}{\pi} \sigma_1(\omega) \quad (8)$$

Here  $c$  is the  $c$ -axis lattice parameter and  $\hbar/e^2 = 4k\Omega$ . Within band theory the total kinetic energy associated with optical transitions within the conduction band is

$$K_{band}(\Omega = \infty) = \int \frac{d^2p}{(2\pi)^2} f(\varepsilon_p) \quad (9)$$

$$(2t_1 \cos p_x - 4t_2 \cos p_x \cos p_y + 8t_3 \cos 2p_x) \approx 0.43 \text{ eV} \quad (10)$$

with less than 2% doping dependence in the range  $x = 0.12 - 0.18$ . Interactions are expected<sup>4,25,26,27</sup> to reduce  $K$  below its band theory value; the amount of the reduction is a measure of the correlation strength<sup>4</sup>.

It is sometimes useful to express measured conductivities in terms of the optical mass  $m^*$  and scattering rate  $\Gamma$  defined via

$$-i\Omega \frac{m^*}{m_{opt}} + \Gamma_{opt} = \left( \frac{\sigma_1(\Omega) + i\sigma_2(\Omega)}{K_{band}} \right)^{-1} \quad (11)$$

Note that we choose to normalize the conductivity to the band theory kinetic energy, Eq 9. A wide variety of other choices have been employed in the literature; different choices lead to different over-all magnitudes for the optically defined mass and scattering rate. We normalize the data to  $K_{band}$  because we are interested in the differences between measurements and the predictions of band theory.

A general expression for the conductivity is complicated<sup>9</sup>. If one makes the assumption that 'vertex corrections' are negligible, then the conductivity becomes  $\sigma = \frac{e^2}{\hbar c} \frac{\Pi^{qp}}{i\Omega}$  (in 'imaginary time') with

$$\Pi^{qp}(\Omega) = T \sum_n \int \frac{d^2p}{(2\pi)^2} \quad (12)$$

$$\mathbf{j}_x(p) \text{Im} G(p, i\omega) \mathbf{j}_x(p) \text{Im} G(p, i\omega + i\Omega)$$

and the Green function  $G$  given as usual by

$$G(p, i\omega) = \int_0^{1/T} d\tau e^{-i\omega\tau} \langle T_\tau d(\tau) d^\dagger(0) \rangle \quad (13)$$

In particular, the dissipative conductivity is

$$\sigma_1^{qp}(\Omega) = \frac{e^2}{\hbar c} \int_{-\infty}^{\infty} \frac{d\omega}{\pi} \frac{[f(\omega) - f(\omega + \Omega)]}{\Omega} \quad (14)$$

$$\int \frac{d^2p}{(2\pi)^2} \mathbf{j}_x(p) \text{Im} G(p, \omega) \mathbf{j}_x(p) \text{Im} G(p, \omega + \Omega)$$

$f$  is the Fermi function. Note that we have chosen units such that the in-plane momentum is dimensionless as is the product  $j_x G$ .

### III. ELECTRON SELF ENERGY

Doped Mott insulators, generally, and cuprate materials, in particular, appear<sup>28</sup> to be characterized by an electronic self energy of unknown origin, which is not small and exhibits a significant temperature and frequency dependence. One widely used model is the "marginal Fermi liquid"<sup>28</sup>. Another class of model self energies, with many similar features, arises from 'spin Fermion models' for materials near magnetic critical points<sup>29,30,31</sup>. The single-site dynamical mean field method leads to a qualitatively similar self energy. The calculations reported below of the optical conductivity use a slightly different self energy, of the form

$$\Sigma(\omega) = \gamma_{imp} + \Gamma(T) \left( 1 - \lambda(T) \frac{\omega_c(\omega_c + i\omega)}{\omega_c^2 + \omega^2} \right) + Z\omega \quad (15)$$

This form is chosen phenomenologically. It represents a self energy with an imaginary part which is small at low frequency and large at high frequency, and without noticeable momentum dependence. This latter assumption is consistent with the photoemission data presented in the previous section.

Here  $\gamma_{imp}$  is a constant scattering rate assumed to come from impurities and the term  $Z\omega$  expresses the effect of renormalizations arising from physics at energies above the highest frequencies considered in the analysis. The remaining 'many body' part of the self energy is taken to be an inverted Lorentzian with frequency scale  $\omega_c$ , and overall strength  $\Gamma$ . The parameter  $\lambda(T)$  controls the crossover from low to high frequency. The key difference from the marginal Fermi liquid form is the presence of a scale,  $\omega_c$ , which will be seen to be quite low. The real and imaginary parts of the model self energy are shown as heavy dashed lines in Figs 3 for the parameters used in the calculation of the conductivity for  $x = 0.17$  (scattering rates extracted from analysis of the optical conductivity are also shown; these will be discussed below). The real part is displayed as a mass enhancement  $m^*/m = 1 - \text{Re} \Sigma(\omega)/\omega$ .

### IV. ANALYSIS OF DATA: KINETIC ENERGY AND MASS ENHANCEMENT

#### A. Overview:

This section presents an analysis of important qualitative features of the observed conductivity, in particular the kinetic energy (Eq 8) and optical mass enhancement (Eq 11). The analysis relies in an essential way on the assumption that in the frequency range of interest both the real and imaginary parts of the measured conductivity arise only from conduction band carriers, with negligible effects of interband transitions. This assumption is clearly correct at very low frequencies, and clearly breaks

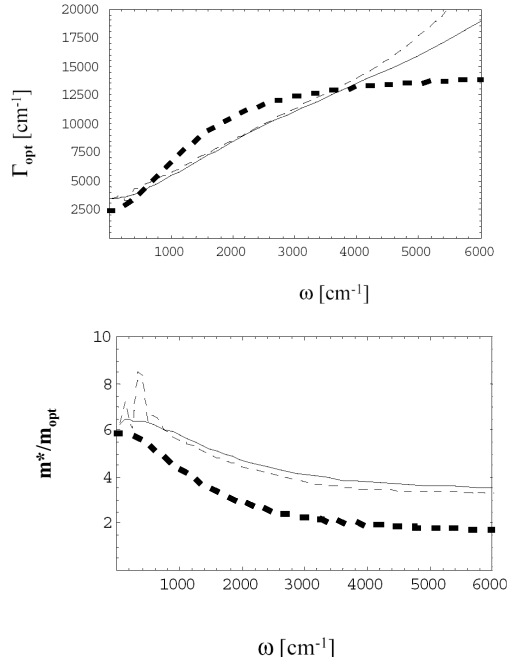
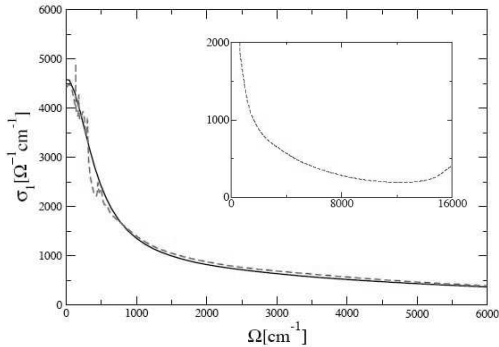


FIG. 3: Scattering rates (upper panel) and mass enhancements (lower panel) derived from room temperature optical data for  $x = 0.17$  material, compared to results of fits and to corresponding single particle rates. Light dashed lines: optically defined scattering rate  $\Gamma_{opt}$  and mass enhancement  $m^*/m_{opt}$  obtained from optical data using Eq 11. Light solid lines:  $\Gamma_{opt}$  and  $m^*/m_{opt}$  obtained by applying Eq 11 to theoretical fit to optical conductivity. Heavy dashed lines: 'single-particle' mass and scattering rate obtained from model self energy used in fits to  $x = 0.17$  room temperature conductivity.

down at sufficiently high frequencies. No clearly defined criterion has appeared in the literature for estimating a frequency below which the conductivity is dominated by the conduction band. The lack of a clear criterion for separating the inter and intra-band contributions to the conductivity is a source of systematic error whose magnitude is at present unknown. The point of view taken here is as follows.

The insulating end-member  $Pr_2CuO_4$  has a conductivity characterized by a gap at  $\omega \approx 1.5eV$ . We believe that it is reasonable to regard this gap as the Mott-Hubbard (or charge transfer) gap and thus to understand the absorption at frequencies  $\Omega \sim 1.5 - 2.5eV$  just above the gap as being dominated by the  $CuO_2$  plane carriers of interest, while an increase at higher frequencies indicates the onset of a strong interband transition. Modest (few percent) doping destroys this large gap and redistributes the  $1.5 - 2.5eV$  absorption to lower frequency<sup>3</sup> while not changing the interband transitions much. We therefore believe that at frequencies less than  $1.5eV$  the observed absorption comes from the  $CuO_2$  plane carriers of inter-



$x=0.17$   $T=300K$  Best fit  $\sigma_2$  compared to data

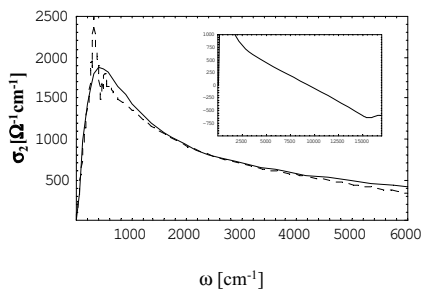


FIG. 4: Measured conductivities compared to theoretical model;  $x = 0.17$  and  $T = 300K$ . Main panels: measured dissipative (upper) conductivity and reactive (lower) conductivities (dashed lines) compared to model calculation (solid lines). Inset: measured conductivities over wide frequency range  $0 - 2eV$ .

est. However, an interband absorption at  $\Omega > 1.5eV$  will produce a contribution to the reactive part of the conductivity at lower frequencies; thus only at frequencies substantially less than  $1.5eV$  will the total conductivity be dominated by the conduction band carriers.

The insets of Fig 4 display the measured conductivities of the  $x = 0.17$  sample over a wide frequency range. The reactive part  $\sigma_2$  displays a zero-crossing at about  $\Omega \approx 1.25eV$ ; we believe that this arises from the absorption feature visible at the high end of the  $\sigma_1$  frequency range. We suggest that the real and imaginary conductivities are dominated by transitions involving the  $CuO_2$  plane carriers only only at frequencies significantly less than  $1eV$ , and we will discuss the data only for frequencies less than  $\omega < 0.75eV$ , and the our main results rely only on frequencies rather less than  $0.5eV$ . As shall be seen below, in this frequency range the analysis yields a consistent picture with conclusions which are insensitive to the precise value of the upper cutoff frequency.

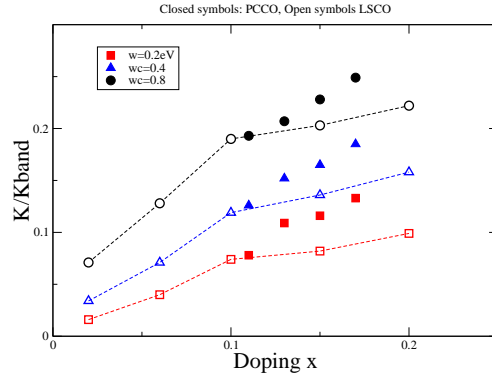


FIG. 5: Solid symbols: kinetic energy, obtained by integrating observed room temperature conductivity for  $Pr_{2-x}Ce_xCuO_4$  films up to several cutoff frequencies and normalizing to the band theory value, plotted against doping. Open symbols: same quantity, obtained from published<sup>3</sup> data on hole-doped  $La_{2-x}Sr_xCuO_4$

## B. Kinetic Energy

The kinetic energy defined in Eq 8 is a fundamental measure of the strength of interactions. If the cuprates were well described by band theory, the low frequency optical conductivity would consist of a narrow 'Drude' peak concentrated at  $\Omega = 0$ , with area leading to a kinetic energy  $K(\Omega)$  which would rapidly approach the value  $K_{band} = 0.43eV$  as  $\Omega$  increases from 0.

The filled symbols in fig 5 show the kinetic energy obtained from the integral of the room temperature conductivity from zero to a cutoff frequency  $\Omega_c$ , normalized to the band value and plotted against doping for different cutoff frequencies. One sees that for all dopings and all relevant frequencies the kinetic energy is a very small fraction of the band value. A linear doping dependence is evident, with slope approximately independent of the cutoff frequency. The linear  $x$  dependence (with slope of the order of unity) and the small intercept are hallmarks of strong correlation or Mott physics<sup>4,25,26,27</sup>.

The figure also shows as open symbols the same quantity obtained from published data<sup>3</sup> for the hole-doped material  $La_{2-x}Sr_xCuO_4$ , where a wider range of dopings are available. One sees that the qualitative features of strong reduction in magnitude and strong doping dependence occur in both electron-doped and hole-doped materials. Interestingly, while the  $La_{2-x}Sr_xCuO_4$  data at low dopings ( $x \leq 0.1$ ) appears as a continuation of the doping dependence observed in  $Pr_{2-x}Ce_xCuO_4$ , in the hole doped material the kinetic energy curves exhibit a pronounced break at about  $x = 0.1$ . The break in slope is not understood and does not, to our knowledge, follow from any theory. Extension to lower dopings of measurements on the electron-doped compounds would be very desirable, as would an improved understanding

of the break in  $x$ -dependence observed in the hole doped materials.

The reasonable correspondences of the kinetic energy magnitudes and doping dependences suggests that the electron doped materials are approximately as strongly correlated as the hole doped ones. The approximately linear doping dependence of  $K$  suggests that the  $U$  value is not strongly doping dependent within the electron-doped family of materials. Both of these observations are in apparent disagreement with recent theoretical studies of electron doped compounds<sup>18,19</sup> suggesting that despite the evident successes of these theories in accounting for the photoemission data, some issues remain in need of clarification.

As doping is increased the optical conductivity increases, but the increase is not uniform in frequency. The upper panel of Fig 6 shows the room temperature kinetic energy difference  $K(x, \Omega) - K(x = 0.11, \Omega)$  for  $x = 0.13, 0.15, 0.17$ . A rapid rise at low frequency is evident, as is an approximate saturation at frequencies greater than about  $0.15eV$ ; in other words, the doped carriers contribute most strongly to the low frequency conductivity. The kinetic energy is also temperature dependent, increasing as  $T$  is decreased. The lower panel of Fig 6 shows the changes in the measured kinetic energy of the  $x = 0.17$  sample as temperature is varied between room temperature and  $25K$ . As the temperature is varied, two effects may occur: a redistribution of spectral weight, arising because scattering rates and mass enhancements have temperature dependences, and a change in the total conduction band spectral weight. Both effects are visible in the lower panel of Fig. 6: the sharp peak near zero frequency arises in part from a decrease in the scattering rate, which narrows the 'Drude peak' leading to a pile-up of spectral weight at low frequency. The saturation at higher frequencies shows that in addition to the rearrangement, there is a net temperature dependent increase, and that this increase affects mainly the low frequency conductivity (since the difference curve is flat above  $\omega \approx .1eV$ ). The change in spectral weight as  $T$  is decreased from room temperature to  $25K$  in the  $x = 0.17$  sample is seen to be of about the same magnitude as the increase in spectral weight as doping is increased from  $x = 0.11$  to  $0.17$

### C. Mass and scattering rate

The dashed curves in Fig. 3 show the mass and scattering rate computed by applying Eq 11 to the  $x = 0.17$  room temperature data for frequencies up to about  $6000 \text{ cm}^{-1} = 0.75eV$ . The light solid curves are obtained from a theoretical fit to  $\sigma$  discussed in detail in the next section. The upturn in the experimental optical scattering rate beginning at about  $6000 \text{ cm}^{-1} \approx 0.75eV$  is caused mathematically by the decrease of  $\sigma_2$  towards its  $1.25eV$  zero crossing. In physical terms, this is a signature that the data at  $\omega \gtrsim 0.75eV$  are significantly affected by an in-

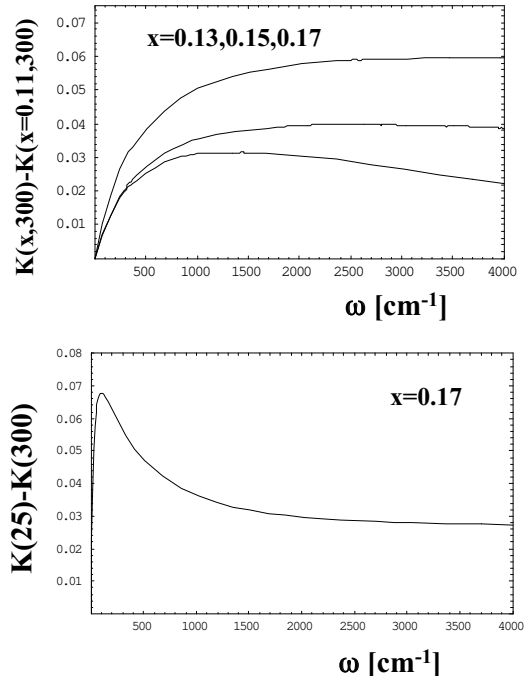


FIG. 6: *Upper panel:* Frequency dependence of difference in room temperature kinetic energy between  $x = 0.11$  sample and  $x = 0.17$  (upper curve)  $x = 0.15$  (middle curve) and  $x = 0.13$  lowest curve. *Lower panel:* Frequency dependence of difference of room temperature and  $T = 25K$  kinetic energy of  $x = 0.17$  sample.

terband transition, rendering an interpretation in terms of mass and scattering rate meaningless. The smooth behavior observed at lower frequencies suggests that for frequencies below about  $1/2eV$  an interpretation in terms of a single band characterized by a mass and scattering rate is reasonable—however, it is possible that even in this regime, interband effects are important. We will return to this issue in the conclusion. The  $\omega < 0.5eV$  data are consistent with an optical scattering rate which is reasonably linear in frequency, as in the hole-doped materials<sup>2,5</sup>.

One sees from Fig. 3 that the optical mass enhancement (relative to band theory) is large, of order 8, even at room temperature, and is strongly frequency dependent. The large mass is simply the restatement of the suppression of kinetic energy discussed above. The characteristic scale of the frequency dependence seen directly in the crossover of the optical mass from its low frequency to its high frequency value is of the order of  $0.25eV$ . The high and low frequency masses are seen to differ by about a factor of two. One may therefore infer that two processes are at work: an over-all suppression of spectral weight (characterized by a frequency scale higher than the highest frequency we analyse) and an additional lower frequency ( $\omega < 0.25eV$ ) effect which enhances the mass by an additional factor of about 2. Analysis (not shown)

of other dopings reveals almost identical behavior.

## V. MODELLING OF DATA

### A. Overview

This section considers the modelling of the optical data within the no-vertex-corrections approximation. It begins with an analysis of the  $x = 0.17$  compound, in which no signatures of density wave order are visible. The next subsection concerns the room temperature behavior as a function of doping (where again no signatures of a density wave gap are evident except perhaps in the  $x = 0.11$  sample), and the final subsection deals with the effect of a density wave gap on the conductivity.

### B. $x=0.17$

This section discusses the modelling of the  $x = 0.17$  optical data. A fundamental assumption is that the conductivity at scales less than  $1eV$  is described by a single band of carriers. The insets in the two panels of Fig 4 suggest that interband transitions become important only above about  $2eV$ . The kinetic energy analysis of the previous section shows that the oscillator strength in the  $\omega < 1eV$  conductivity is substantially less than is predicted by band theory. An analysis involving strong correlations is therefore needed. Here it will be assumed, consistent with the 'single-site dynamical mean field approximation'<sup>10</sup> and with many other works<sup>28,29,30,31</sup>, that the main effect of the correlations is to produce an electron self energy which may be large and strongly frequency dependent.

The solid lines in Fig. 4 show the results of theoretical calculations based on Eqs 14 and 5, with  $\Gamma = 0.9eV$ ,  $\lambda = 0.83$ ,  $Z = 0.5$  and  $\omega_c = 0.17eV$ . The agreement with data (dashed lines) is reasonable. The real and imaginary parts of the electronic self energy are shown as heavy dashed lines in Fig. 3. The self energy is characterized by a surprisingly low frequency scale ( $0.17eV$ ) and by a very large magnitude. The high frequency limit of the imaginary part of the self energy is found to be frequency independent, with a value  $\approx 1.5 eV$ , comparable to the band width. The low frequency mass enhancement is correspondingly large (of order 6), and arises mostly from processes acting at the relatively low scale set by  $\omega_c$ . The fits involve a function of several parameters, and it is therefore difficult to say precisely what are the uncertainties in the resulting values. However,  $\Gamma$  sets the rate at which the  $\omega > 3000cm^{-1}$  conductivity drops with frequency,  $Z$  sets the magnitude of the conductivity in the high frequency regime,  $\lambda$  sets the value at low  $\omega$ , and  $\omega_c$  determines the scale at which the behavior crosses over from low to high frequencies. Significant (more than 10%) changes in any one of these parameters leads to noticeable decreases in the quality of the fits.

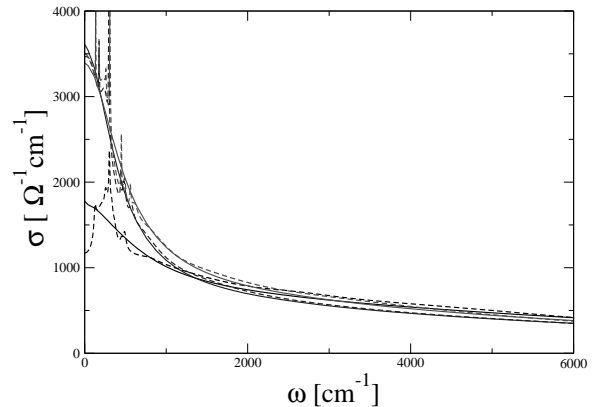


FIG. 7: Real part of measured room temperature conductivity (dashed lines) compared to theoretical model (solid lines) for  $x = 0.11, 0.13, 0.15$ .

It is evident from Fig 3 that the optically defined mass and scattering rates are not faithful representations of the single particle mass and scattering rates. In particular the calculated optical scattering rate is much more nearly linear than is the imaginary part of the model single-particle self energy, while the assumed single particle mass drops off more quickly than the optically defined one.

### C. Doping dependence

This subsection summarizes the results of fitting the room temperature conductivities with the quasiparticle-only model. Fig 7 shows the measured room temperature conductivities and the best-fit calculated conductivities (solid lines) at the other available dopings  $x = 0.11, 0.13, 0.15$ . Fig 8 shows the single-particle mass enhancement inferred from these fits. The parameters are indicated in Table I.

Fig. 8 shows that for  $x = 0.13, 0.15$  and  $0.17$  there is a negligible doping dependence of  $m^*$  at high frequencies while there is a characteristic, low frequency scale, below which the mass sharply increases, in a manner which depends on doping. This is a restatement, in the language of single particle mass, of the observation made above that the effect of doping is to add spectral weight at low frequencies.

The  $x = 0.11$  sample is seen to deviate from the monotonic behavior. We will argue below and in a companion paper that this deviation is associated with the presence of antiferromagnetism even at room temperature.

For all dopings, the zero frequency (Fermi surface) mass enhancements implied by the analysis are very large. As seen in the Table, this implies quasiparticle velocities substantially suppressed relative to band velocities.

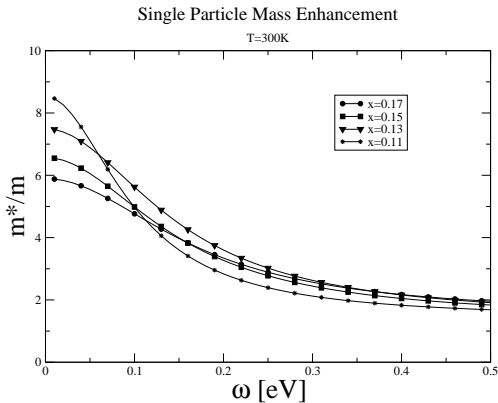


FIG. 8: Frequency dependent single particle mass enhancement  $m^*/m = 1 - \text{Re}\Sigma(\omega)/\omega$  inferred from self energy only analysis of room temperature conductivity.

TABLE I: Self energy parameters and associated velocity renormalization implied by self-energy-only analysis of room temperature conductivity

Doping	$\Gamma$ [eV]	$\lambda$	$\omega_c$ [eV]	$Z$	$v^*/v_{band}$
0.11	0.95	0.75	0.1	0.41	0.12
0.13	1.1	.83	0.15	0.41	0.13
0.15	0.98	0.79	0.15	0.41	0.15
0.17	0.9	0.83	0.17	0.5	0.17

#### D. Low Temperature analysis

Figs 9 show data and model conductivities at low temperature (25K). Again the agreement is reasonably good, although as can be seen from the inset the model underestimates the mass enhancement and overestimates the scattering rate at low frequencies. The 'best fit' parameters for the low frequency data are  $\Gamma = 0.75\text{eV}$ ,  $\lambda = 0.98$ ,  $Z = 0.4$  and  $\omega_c = 0.12\text{eV}$ . The decrease in  $Z$  reflects the increase in conduction band kinetic energy; the increase in  $\lambda$  reflects the smaller value of the  $dc$  scattering rate; the decrease in  $\Gamma$  reflects the smaller value of the high frequency optical scattering rate (more rapid decrease of  $\sigma_1$ ) and the decrease in  $\omega_c$  reflects the lower frequency and more rapid crossover of the data from high to low frequency. The actual value of the high frequency conductivity has very little temperature dependence; thus in this parametrization changes in the parameters  $Z$  and  $\Gamma$  controlling the high frequency conductivity must compensate each other. Figs. 10 show the single particle and optically defined mass and scattering rate following from the fits to the low temperature data. The qualitative behavior is very similar to that of the higher temperature results.

Difficulties arise in applying this analysis to the low  $T$  behavior of the lower  $x$  samples. The issue is most clearly revealed by examination of the data for  $x = 0.13$  sam-

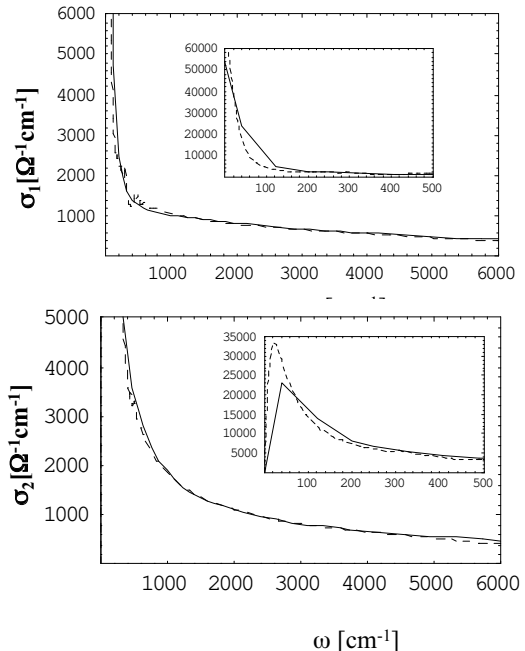


FIG. 9: Main panels: measured dissipative (upper) conductivity and reactive (lower) conductivities (dashed lines) compared to model calculation (solid lines) for  $x = 0.17$  and  $T = 25\text{K}$ . Inset: expanded view of low frequency regime

ple. Comparisons of the dashed and dotted lines in Fig. 11 shows that as temperature is decreased the dissipative conductivity does not simply shift towards lower frequency, as does the conductivity of the  $x = 0.17$  material. Instead, an upward shift occurs in frequency, as expected if a density wave gap opens up. The conductivity of this material will be discussed in terms of antiferromagnetism in a companion paper.

## VI. COMPARISON TO PHOTOEMISSION

The parameters obtained from the fits to the optical data make predictions for photoemission spectra. To facilitate comparison to experiment we plot these as energy dispersion curves ('EDC') which are the imaginary part of the electron Green function, plotted as a function of energy at fixed momentum. The two panels of Fig. 12 show EDC traces calculated using the self energy which best fits the room temperature  $x = 0.17$  optics calculation.

The 'no-vertex-corrections' modelling of the conductivity requires that the quasiparticle mass enhancement be very large in order to account for the suppression of spectral weight relative to band theory. The predicted Fermi velocity renormalizations are given in the last column of



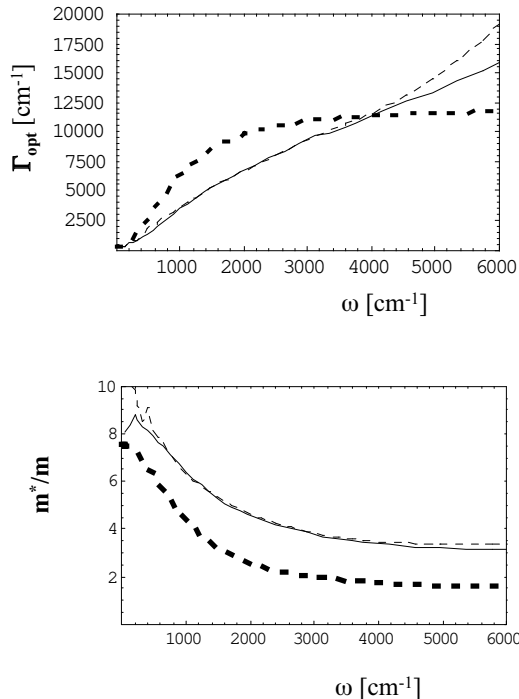


FIG. 10:  $T = 25K$  scattering rate (upper panel) and mass enhancement (lower panel) derived from optical data (light dashed line), from theoretical fits to optical data for the  $x = 0.17$  sample (light solid line) compared to 'single-particle' mass and scattering rate obtained from model self energy ( $\hbar\omega$ )

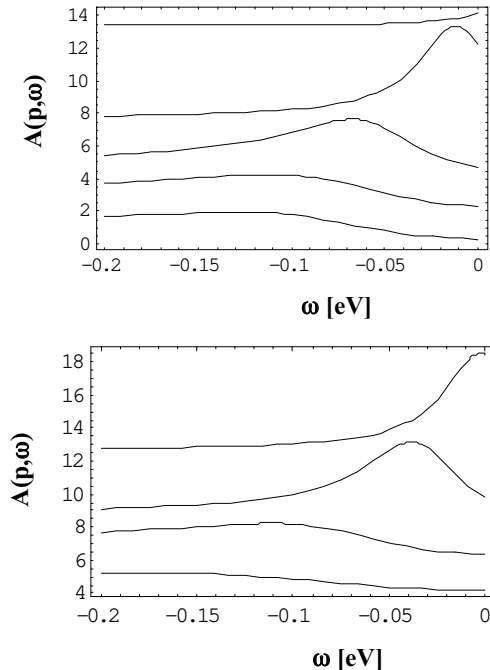


FIG. 12: Energy dispersion curves (electron spectral function as function of energy for fixed momentum) calculated for 300K best-fit optical parameters. Top panel: momenta along zone face  $p = (\pi, (0, 0.1, 0.2, 0.3, 0.4) * \pi)$  Lower panel: zone diagonal,  $p = 0.4, 0.6, 0.8, 0.9 * \pi, \pi)$ .

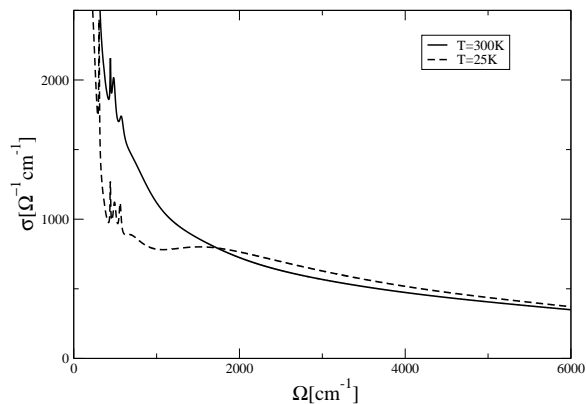


FIG. 11: Measured conductivity for  $x = 0.13$  sample at room temperature and low temperature.

the Table. These imply zone-diagonal Fermi velocities of order  $0.5eV - \text{\AA}$ , as may be seen directly from the dispersions of the peaks in Fig. 12. The velocities have been directly measured in photoemission experiments<sup>22</sup> and are found to be much larger, of order  $1.5 - 2eV - \text{\AA}$ , as may be seen in Fig 2. This dramatic inconsistency shows that the self-energy-only model is not applicable

to the electron-doped cuprates. In Fermi-liquid terms, a rather large vertex correction is important. Theories of the conductivity<sup>6,30,31</sup> which do not include this factor seem unlikely to be directly applicable to the actual materials.

## VII. CONCLUSION

We have presented a detailed analysis of the optical conductivity of a series of films of electron-doped cuprates. We have shown, via an analysis of the kinetic energy, that the materials are approximately as strongly correlated as the corresponding hole-doped systems. We have performed detailed modelling of the observed optical spectrum using a self energy which depends on frequency only. The essential assumption underlying this analysis is that at relevant frequencies the real and imaginary parts of the measured conductivity are dominated by the response of mobile carriers moving in the band structure inferred from band theory calculations and scattered by some frequency and temperature dependent scattering mechanism. The optical response at low frequencies corresponds to a large (factor 6–10) mass enhancement relative to band theory; within the scattering only model this

mass enhancement would imply a photoemission spectrum characterized by a velocity much lower than is actually observed. Thus we conclude that the doping dependent suppression of optical oscillator strength cannot be due solely to local physics of the sort considered in the single-site dynamical mean field theories of doped Mott insulators or in a variety of phenomenological models. As an aside we find that the scattering rate inferred from an 'extended Drude' analysis of the conductivity need not be a particularly faithful representation of the underlying single particle scattering rate (see Fig. 3).

The modelling was performed on the assumption that at frequencies less than  $\approx 0.5eV$  the real and imaginary parts of the measured conductivity arise from scattered conduction band carriers. For frequencies greater than about  $0.75eV$  this assumption was shown to be untenable: a high frequency interband transition produces a negative contribution to  $\sigma_2$ , leading to an unphysical upturn in the scattering rate (see Fig. 3 and section IV-C). Although we presented qualitative arguments that at frequencies less than  $1eV$  the absorptive part of the conductivity is due to conduction band carriers, these arguments are not conclusive. It is possible that even at lower frequencies, interband transitions could appear, invalidating the analysis presented here. If this occurred, some of the optical oscillator strength presently assigned to the conduction band would be reassigned to an irrelevant transition; the optical masses would therefore be increased, worsening the discrepancy between optical and photoemission masses. We therefore suspect that our main finding, of a large discrepancy between the predictions of a self-energy-only theory and the photoemission and optical data, is robust.

Taken together, the available data present the following conundrum. Optical spectral weight is proportional to a carrier density times a charge squared divided by a carrier mass:  $K \sim \frac{n_{eff}e_{eff}^2}{m_{eff}}$ . Two conventional interpretations of a small spectral weight are a small number of carriers or a large carrier mass. The photoemission measurements reveal (at least for large dopings where density wave effects are absent) a large Fermi surface, consistent with band theory, and ruling out a simple small carrier number picture. Hall effect measurements<sup>32</sup> also indicate for optimally doped materials a carrier number reasonably consistent with the band theory value. A large body of theoretical work<sup>10,28,29,30,31</sup> relates the optical conductivity to an essentially local scattering rate and the spectral weight suppression to an enhanced quasi-particle mass. Our analysis shows that these theories require a mass enhancement larger by a factor of at least 4 than is directly observed in photoemission. One is therefore forced to look to a renormalization of the 'effective charge'. In Fermi liquid language, this renormalization is expressed as a vertex correction or Landau parameter, so one must assume that the Mott correlations are expressed by a vertex correction which diverges as the doping decreases. Unfortunately, the most straightforward implementation of the vertex correction idea strongly disagrees with measurements of the magnitude of the superconducting penetration depth<sup>(14)</sup>. Construction of a viable theory of the optical conductivity of this (and perhaps other) strongly correlated two dimensional materials remains an important open problem.

*Acknowledgements:* AJM acknowledges support from NSF-DMR-0431350 and the CNRS.

- 
- <sup>1</sup> A. Damascelli, Z. Hussain, and Z.-X. Shen, *Rev. Mod. Phys.* **75**, 473-541 (2003)
- <sup>2</sup> J. Orenstein, G. A. Thomas, A. J. Millis, S. L. Cooper, D. H. Rapkine, T. Timusk, J. V. Waszczak, *Physical Review* **B42**, 6342-62 (1990).
- <sup>3</sup> S. Uchida, *Phys. Rev.* **B43**, 7942-54 (1991).
- <sup>4</sup> "Optical Conductivity and Correlated Electron Physics", A. J. Millis, in *Strong Interactions in Low Dimensions*, D. Baeriswyl and L DeGiorgi, eds (Springer Verlag: Berlin 2004).
- <sup>5</sup> Z. Schlesinger, R. T. Collins, F. Holtzberg, C. Feild, S. H. Blanton, U. Welp, G. W. Crabtree, Y. Fang, and J. Z. Liu, *Phys. Rev. Lett.* **65**, 801-804 (1990).
- <sup>6</sup> C. M. Varma and E. Abrahams, *Phys. Rev. Lett.* **86**, 4652 (2001).
- <sup>7</sup> P. W. Anderson, *Science* **280**, 480-1 (2000).
- <sup>8</sup> D. van der Marel et. al., *Nature* **425** 271-4 (2003).
- <sup>9</sup> A. J. Millis and H. D. Drew, *Phys. Rev.* **B 67**, 214517/1-7 (2003).
- <sup>10</sup> A. Georges, G. Kotliar, W. Krauth, and M. J. Rozenberg, *Rev. Mod. Phys.* **68**, 13-125 (1996).
- <sup>11</sup> M. Imada, A. Fujimori and Y. Tokura, *Rev. Mod. Phys.* **70** 1039-1263 (1998).
- <sup>12</sup> L. B. Ioffe and A. I. Larkin, *Phys. Rev.* **B39**, 8988-8999 (1989).
- <sup>13</sup> M. J. Rozenberg, G. Kotliar, H. Kajueter, G. A. Thomas, D. H. Rapkine, J. M. Honig, and P. Metcalf, *Phys. Rev. Lett.* **75**, 105-108 (1995).
- <sup>14</sup> L. B. Ioffe and A. J. Millis, *Journal of Physics and Chemistry of Solids* **63** 2259-68 (2002); see also A. J. Millis, S. M. Girvin, L. B. Ioffe and A. I. Larkin, *J. Phys. Chem. Sol.* **59** 1742-4 (1998).
- <sup>15</sup> Y. Onose, Y. Taguchi, K. Ishizaka, and Y. Tokura, *Phys. Rev. Lett.* **87**, 217001 (2001).
- <sup>16</sup> Y. Onose et al., *Phys. Rev. B* **69**, 024504 (2004).
- <sup>17</sup> A. Zimmers, J.M. Tomczak, R.P.S.M. Lobo, N. Bontemps, C.P. Hill, M.C. Barr, Y. Dagan, R.L. Greene, A.J. Millis, C.C. Homes, cond-mat/0406204.
- <sup>18</sup> C. Kusko, R. S. Markiewicz, M. Lindroos, and A. Bansil, *Phys. Rev.* **B66**, 140513 (2002).
- <sup>19</sup> B. Kyung, V. Hankevych, A.-M. Dar, and A.-M. S. Tremblay *Phys. Rev. Lett.* **93**, 147004 (2004) and D. Sncal and A.-M. S. Tremblay *Phys. Rev. Lett.* **92**, 126401 (2004).
- <sup>20</sup> O. K. Andersen, A. I. Liechtenstein, O. Jepsen and F. Paulsen, *J. Phys. Chem. Solids* **56**, 1573 (1995).
- <sup>21</sup> S. Massida, N. Hamada, J. Yu, and A. Freeman, *Physica*

- (Amsterdam) 157C, 571–574 (1989)
- <sup>22</sup> N. P. Armitage et. al. Phys. Rev. Lett. **88**, 257001 (2002).
- <sup>23</sup> T. Claesson, M. Mansson, C. Dallera, F. Venturini, C. De Nadai, N. B. Brookes and O. Tjernberg, Phys. Rev. Lett. **93** 136402/1-4 (2004).
- <sup>24</sup> F. C. Zhang and T. M. Rice, Phys. Rev. **B37** 3759 (1988).
- <sup>25</sup> A. J. Millis, S. Coppersmith, Physical Review **B42**, 10807-10 (1990).
- <sup>26</sup> H. J. Schulz, Phys. Rev. Lett. **64**, 2831 (1990).
- <sup>27</sup> C. A. Stafford and A. J. Millis, Phys. Rev. **B48**, 1409 (1993).
- <sup>28</sup> C. M. Varma, E. Abrahams, S. Schmidt-Rink and A. Ruckenstein, Phys. Rev.Lett. **63** 1936 (1989).
- <sup>29</sup> C. Jiang, E. Schachinger, J. P. Carbotte, D. Basov, and T. Timusk, Phys. Rev. **B54**, 1264–1272 (1996).
- <sup>30</sup> Branko P. Stojkovic and David Pines, Phys. Rev. **B55**, 8576–8595 (1997)
- <sup>31</sup> R. Haslinger, Andrey V. Chubukov, and Ar. Abanov, Phys. Rev. **B63**, 020503/1-4 (2001) see also Adv. Phys. **52** 119 (2003).
- <sup>32</sup> Y. Dagan, M.M. Qazilbash, C. P. Hill, V. N. Kulkarni, and R. L. Greene, Phys. Rev. Lett. **92**, 167001 (2004).